Chapter 5

The influence of the surface topography on the magnetization dynamics in soft magnetic thin films

We report on the influence of the surface roughness on the magnetization dynamics of soft magnetic nanocrystalline Fe-Zr-N thin films. The substrates used in this study were Si-oxide, a thin polymer layer and a thin Cu layer. We have deposited the samples under the same conditions. The substrate temperature during deposition was around -25ºC, ensuring a fine nanocrystalline state in all samples. The demagnetizing factors N_{xx}, N_{yy} and N_{zz} due to sample roughness were calculated based on AFM analysis of the surface topography. A clear correlation between sample roughness and the width of the high frequency response is observed. The local random demagnetizing field created by the nanocrystalline structure is responsible for the positive shift of the ferromagnetic resonance (FMR) frequency. Additionally, a pronounced effect of line broadening is induced by the surface topography at large wavelength. We have obtained a reasonable agreement between the values of the average local demagnetizing field $N4\pi M_S$ as calculated from the AFM scans and the halfwidth of the local field distribution calculated from the frequency-dependent complex permeability measurements.

5.1. Introduction

The development of new technologies related to magnetic recording industry and the spread of wireless communication systems is an important incentive to focus on magnetic materials which can be used in high frequency applications [1, 2]. Depending on the application, the requirements which must be satisfied by these materials can vary considerably. For instance, in order to improve the design of a high frequency inductor we can use a soft magnetic material with high ferromagnetic resonance (FMR) frequency. A narrow FMR line and a high real component of the magnetic permeability are desirable in this case. Somewhat different properties must be satisfied by the materials which are used for band stop filters which depend on the absorption of microwave power at the FMR frequency; the position and the width of the FMR line must be adjustable depending on the working frequency range. Therefore it is desirable to obtain a magnetic material which can be used for a large range of frequencies. The high frequency properties of this material will be artificially modified by changing the extrinsic parameters of the samples.

One obstacle which must be removed in order to have this "tunable" magnetic material is the magnetocrystalline anisotropy. This can be done by choosing a nanocrystalline structure with random orientation of the grains [3, 4]. An important factor is also the saturation magnetization M_S. In almost all high frequencies applications involving a ferromagnetic material, an increase of M_S leads to an improvement of the physical property of interest. We take the examples above: (i) for an inductor, a higher M_S increases the inductance and the frequency range, and (ii) for a stop band filter higher M_S means higher power absorption.

In this chapter we present a study of the high frequency response of Fe-Zr-N thin films with a nanocrystalline structure and uniaxial induced anisotropy, where we concentrate on a variation of the substrate on which the films are deposited. We show that substrate roughness induces significant changes of the magnetization dynamics. The FMR frequency distribution is very broad and the average FMR frequency is shifted upward corresponding to an extra field of about 35 Oe for the sample deposited on the roughest substrate. We discuss the origin of both the broadening and the frequency shift.

5.2. Experimental

The deposition method used for the production of the samples was DC reactive sputtering in an $Ar+N_2$ gas mixture. We have kept the same sputtering parameters for all samples used in this investigation. The target was a Fe-Zr alloy with a Zr concentration of only 1%. This small amount of Zr has the role of increasing the nitrogen uptake and may act also as a thermal stabilizer in subsequent treatments. However, only the first Zr-related property was considered for this study

since no thermal treatments were done. The sample thickness was 110 nm for all samples. Another important factor in sample deposition was the temperature of the substrate. All samples were produced at temperatures below -20ºC producing grain sizes around 2 nm, see Table 1. More details about this deposition technique are given elsewhere [5, 6]. In order to change the topography of the samples, we have used the following substrates: (i) Si-oxide, (ii) Si covered with a thin organic layer and (iii) Si-oxide covered with a 300 nm Cu layer. The second substrate was prepared by applying a uniform layer of dinitro cellulose in a solution of amilacetate and acetone (colodium) with a thickness of 1μm.

In order to measure the average grain size and the nitrogen content, the structure was investigated by XRD. We have used for these purposes the Scherrer formula and the relation between lattice constant and nitrogen concentration [5]. Based on the average lattice parameters, the samples A and B had a nitrogen content of 16%. For the sample deposited on Cu the XRD technique was ineffective because of the superposition of the diffraction peaks of Cu substrate and sample. Because the substrate temperature of -24ºC was almost the same as for the other samples, we expect that the grain size and the nitrogen content will be similar. The surface topography of the samples was analyzed with an atomic force microscope (AFM).

The DC magnetic properties were studied with a vibrating sample magnetometer (VSM). We have measured the high frequency magnetic response with a single-coil system connected to a network analyzer [7]. An electron spin resonance (ESR) set-up working in X-band (9.4 GHz) was also used.

Table 5.1 Structural parameters of the samples; *w* is the root mean square roughness amplitude.

Sample name	A	B	C
Substrate	Si(100)	Organic	Cu (300nm)
Dep. Temp. (°C)	-27	-32	-24
Grain size (nm)	2	2	~2
N (at%)	16.1	14.5	~15
w (nm)	0.3	2.3	5.1

5.3. Results

5.3.1. Surface morphology

The AFM scans of samples B and C are presented in Fig. 5.1.a,b. We have observed that the film surface roughness increases going from sample A (Si-oxide substrate, not shown here) via sample B (organic substrate) to sample C (Cu

substrate). The substrate morphology revealed similar features with those of the film surface upon 100 nm deposition of Fe, indicating replication of the substrate topology. This was observed on AFM scans of those regions of the samples which were not covered by the magnetic material due to the substrate holder shadowing effect. The orientation of the coordinate system used here is given in Fig. 5.2.

Indeed, the height-difference correlation function $g(x)=<[h(x)-h(0)]^2>$ in the fast scan direction was computed (and averaged along the z-direction or slow scan direction), where $h(x)$ is the surface height at lateral position x on the surface relative to the mean surface height. A typical example is shown in Fig. 5.1c. For a self-affine rough morphology we have [8]:

$$g(x) = \rho^2 x^{2H} \quad \text{for } x << \xi \tag{5.1}$$

$$g(x) = 2w^2 \quad \text{for } x >> \xi \tag{5.2}$$

with ξ the lateral correlation length, $w = \sqrt{< h^2 >}$ the rms roughness amplitude, and $\rho \propto w/\xi^H$ the average local surface slope. Therefore, the rms roughness amplitude w can be obtained from the regime of saturation of $g(x)$ (where its measurement requires a scan size >10ξ), while a double log-plot at shorter length scales yields the roughness exponent H (Fig. 5.1c). As H decreases, the surface becomes more irregular (jagged) at short length scales ($x << \xi$).

Finally, the correlation length ξ is given by the intersection of power-law and saturation lines by $\xi = (2w^2/\rho^2)^{1/2H}$. Measurement of the roughness parameters w, ξ, and H allows further calculation of the demagnetizing factors.

The roughness analysis for the sample shown in Fig. 5.1b-c (Fe/Cu; scan size 3000 nm) yielded H=0.92±0.05, w=5.1 nm, and ξ=78.2 nm. For the sample B shown in Fig. 5.1a (Fe-Zr-N/polymer) the rms roughness amplitude is not yet saturated over scan sizes of 6000 nm or more due to the presence of the hillocks as Fig. 5.1a, yielding w=2.3 nm. These hillocks have lateral base dimensions L≈400 nm with average height Δ≈5nm and are very likely to dominate magnetic film characteristics. Finally, for the Fe films deposited onto Si-oxide the obtained rms roughness amplitude was ≈0.3nm excluding thus any significant contribution of surface/interface roughness onto magnetic properties.

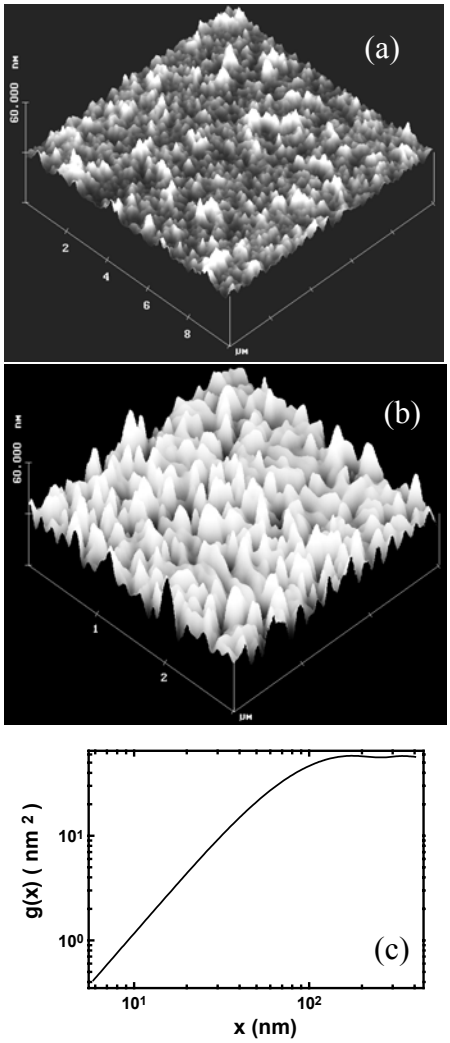

Fig. 5.1. AFM scans of the samples B (a) and C (b); height difference correlation function corresponding to sample C

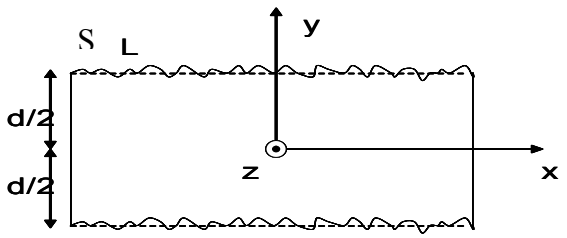

Fig. 5.2 The cross section of the film lying in the x-z plane; d is the film thickness; *S* is the film boundary defined by *d/2+h(x,z)*

For the film shown in Fig. 5.1b-c the demagnetizing factors are calculated as follows. If we assume isotropic and translation invariant random roughness in two dimensions, then the (average) demagnetizing factor corresponding to the whole surface is given by [9]:

$$N_{xx} = \frac{(2\pi)^4}{4dA}\int d^2k\left[\left\langle\left|h_f(k)\right|^2\right\rangle + \left\langle\left|h_s(k)\right|^2\right\rangle - 2e^{-dk} <h_f(k)h_s(k)>\right]k \quad (5.3)$$

with $h_f(k)$ and $h_s(k)$ respectively the two-dimensional Fourier transform of the film surface and substrate height fluctuations. A is the average macroscopic flat surface area. The approximation is made that everywhere the spins are parallel. For conformal to substrate film surface roughness, or $h_f(k) \equiv h_s(k)$, Equation (5.3) yields:

$$N_{xx} = \frac{(2\pi)^4}{2dA}\int d^2k\left\langle\left|h_f(k)\right|^2\right\rangle k\left[1 - e^{-dk}\right] \quad (5.4)$$

In order to calculate the demagnetizing factor we assume a simple Lorentzian model for the roughness spectrum $\left\langle\left|h_f(k)\right|^2\right\rangle$ [10]:

$$\left\langle|h_f(k)|^2\right\rangle = \frac{A}{(2\pi)^5}\frac{w^2\xi^2}{(1+ak^2\xi^2)^{1+H}} \quad (5.5)$$

with $a = (1/2H)[1-(1+aQ_c^2\xi^2)^{-H}]$ if 0<H<1 (power-law roughness), and $Q_c = \pi / a_o$ with a_o of the order of atomic dimensions. For other self-affine roughness correlation models see also Ref. 11.

For the roughness parameters H=0.92, w=5.1 nm, and ξ=78.2 nm of the sample C deposited onto Cu (Fig. 5.1b-c) we obtain $N_{xx} = N_{zz} = 3.6x10^{-3}$. The diagonal components of the demagnetizing factor are determined by the relations $N_{xx} = N_{zz}$ (isotropic roughness) and $N_{xx} + N_{yy} + N_{zz} = 1$.

For sample B shown in Fig. 5.1a the demagnetizing factor was estimated using a different approach since the surface has a different configuration, as we already mentioned. Here we can approximate the large wave length features with uniform magnetized ellipsoids having the long axis equal with L and the short axis equal with Δ. We obtain $N_{xx}=N_{zz}\cong 1x10^{-3}$ [12].

5.3.2. Magnetic characterization

We present in Fig. 5.3 the hysteresis loops of the samples measured with applied field, H_{DC}, parallel and perpendicular to the easy axis (EA), respectively. In the coordinate system chosen the *Oy* axis is perpendicular to the surface, EA is along the *Oz* axis and the rf field is along *Ox*.

All samples measured in the EA orientation had values of the remanent magnetization almost equal to saturation values. This shows that a stable single-domain magnetic structure is formed even when the external field is zero. The initial permeability is larger than $N_{xx}^{-1} = N_{zz}^{-1}$, i.e. the system does not form domains in order to keep the internal field zero, which would minimize the magnetostatic energy. The reason for this behavior is that the spins cannot follow all topography variations due to the strength of the exchange interactions.

In principle the anisotropy field, H_K, can be extracted from the hysteresis loops measured in the hard direction. We could estimate reliably H_K in this way only for sample *A,* which has a coercive field of about 1Oe. For samples B and C, where the coercivity is much higher, we estimate that H_K does not exceed 25 Oe. A better estimation of H_K was obtained using FMR at 9.4 GHz, see Table 5.2.

For an example of the X-band measurements, see Fig. 5.4. As pointed out by Oates et al. [17] the output signal of an ESR spectrometer is composed of absorption and dispersion lines. In the ideal case only the absorption line should be observed.

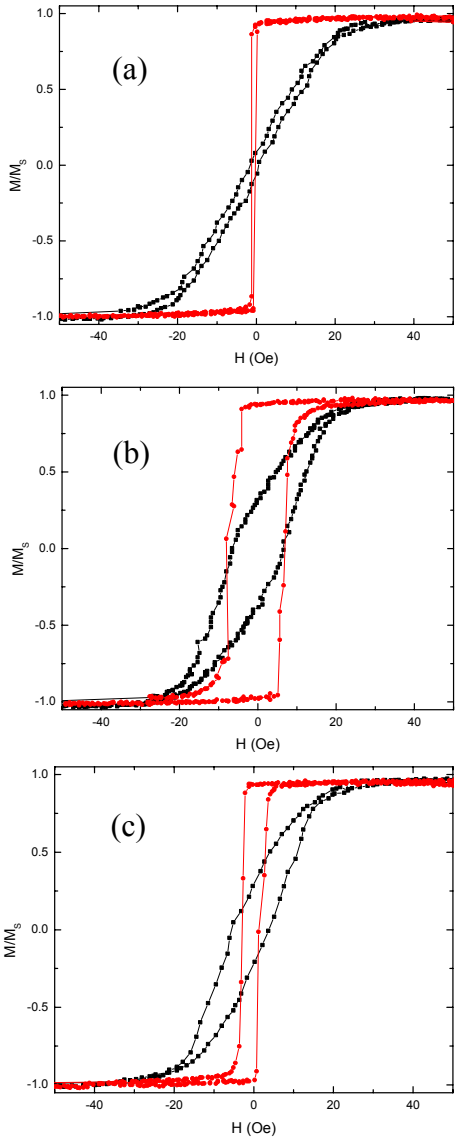

Fig. 5.3 Hysteresis loops of the samples A - a, B - b and C - c; measurements performed parallel and perpendicular to the easy axis.

Sample	A	B	C
$H_{K\text{-}VSM}$ (Oe)	23	<25	<25
$H_{K\text{-}FMR}$ (Oe)	23	13	29
$H_r=(H_{r1}-H_{r2})/2$ (Oe)	625	613	578
ΔH_{FMR} (Oe)	14.5	35	92
$4\pi M_S$ (kG)	15.6	15.4	16
f_R (GHz)	1.95	2.33	2.92
H_K+H_{Shift} (Oe)	28	39	54
H_0 (Oe)	0	24.6	44
α_{field}	0.0023	0.0054	0.014
$\alpha_{frequency}$	0.01	0.023	0.025
$N_{xx}4\pi M_S$ (Oe)	-	15	55

Table 5.2 Magnetic parameters: anisotropy field measured with *VSM* ($H_{K\text{-}VSM}$) and X-band FMR ($H_{K\text{-}FMR}$), H_r the average resonance field and the linewidth ΔH_{FMR} from X-band measurements, the resonance frequency f_R obtained from permeability spectra; the rest of the parameters are explained in the text.

By introducing a dispersion component we can fit the signal correctly and determine the resonance field H_R together with the field line-width ΔH. The analysis can be performed using the following formula:

$$y = \frac{a\left(\frac{H_R - H}{\Delta H_R}\right) + 9b - 3b\left(\frac{H_R - H}{\Delta H_R}\right)^2}{\left[3 + \left(\frac{H_R - H}{\Delta H_R}\right)^2\right]^2} \tag{5.6}$$

where a and b are the amplitudes of the absorption and dispersion signals, respectively. An example is presented in Fig. 5.5. As already mentioned, H_K was calculated from the half of the difference between H_R obtained with Eq. 5.6 for the situation when the external field is oriented in the plane of the sample perpendicular to EA and parallel to EA, see Fig. 5.4. The values of $\Delta H/2$ are included in Table 2.

The values of $4\pi M_S$ as given in Table 5.2 are calculated assuming g=2.1 [13] for all samples. In fact, for the estimation of $4\pi M_S$ we have taken into account not only the X-band measurements, but also the frequency-dependent permeability (see later). Since all samples were deposited in almost the same sputtering conditions, it is to be expected that the saturation magnetization does not vary too much.

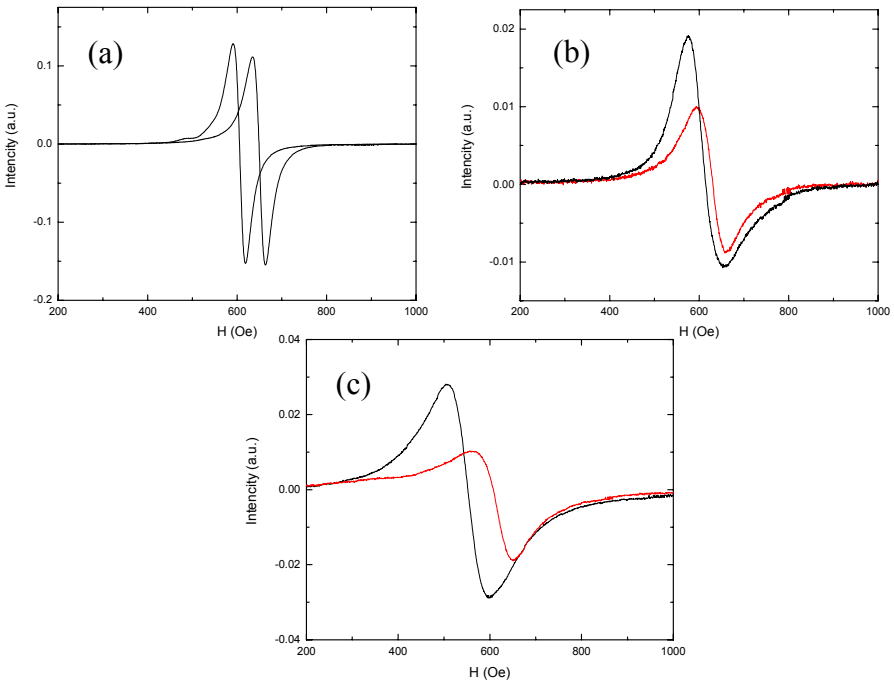

Fig. 5.4 ESR spectra of samples A – a, B – b and C – c measured with H_{DC} in the plane of the sample, parallel and perpendicular to the EA.

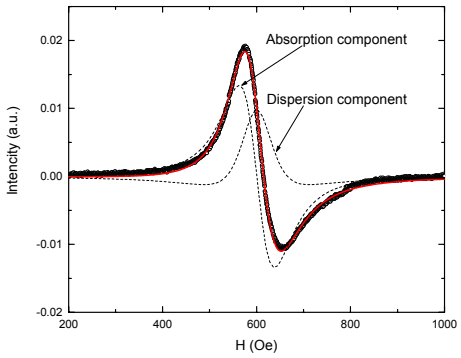

Fig. 5.5 ESR measurement for sample B: Experimental data is represented by circles, the absorption and dispersion components are indicated by arrows and the fit of the experimental data is represented by the continuous line.

The frequency-dependent permeability of the samples is presented in Fig. 5.6. A clear difference can be observed between the sample deposited on Si and the samples deposited on the other substrates. While sample A presents a relatively sharp resonance with a $\Delta\omega \cong 520$ MHz, the resonances in samples B and C were very broad, with *FWHM* larger than 1 GHz. This increase of the linewidth is accompanied by an increase of the average resonance frequency, corresponding to the zero crossing of the real part of the permeability μ'. It is evident that a correlation exists between the sample roughness and the high frequency response.

As a *first method* of analysis, we suppose that in sample B and C the local demagnetizing field is varying from one region to another and has the following position dependence: $H_{dz}=H_0 cos(kz)=H_0 cos(\theta)$, where $\theta \in [0,\pi]$ and $2\pi/k$ is appreciably larger than the coherence length ξ. For coherent rotation of spins, the dynamics of the system can be reasonably well described by the Landau-Lifshitz equation [14]. Details about how this equation is solved under proper assumptions are given elsewhere [15, 16]. We note that no eddy current effects are expected because the chosen thickness is much smaller than the skin depth.

In order to fit our frequency-dependent spectra, we have considered the following expression for the total local field:

$$\boldsymbol{H}_T = \boldsymbol{H}_{DC} + \boldsymbol{H}_{RF}(t) + \boldsymbol{H}_K - \boldsymbol{H}_{dem} + \boldsymbol{H}_d + \boldsymbol{H}_{Shift} \qquad (5.7)$$

where $\boldsymbol{H}_{dem}=(0,4\pi M_S,0)$ is the demagnetizing field in the absence of surface roughness and $\boldsymbol{H}_d=(H_{dx},H_{dy},H_{dz})$ is the local demagnetizing field, which should not be confused with the average value calculated on basis of the (N_{xx}, N_{yy}, N_{zz}) coefficients. $\boldsymbol{H}_{Shift}$ is an extra field needed to obtain a good fit of the experimental data. The frequency-dependent magnetic response of the system is obtained by calculating the envelope of the permeability $\mu=\mu(\theta)$ over a period of the oscillating $\boldsymbol{H}_d$. For this analysis we have chosen n=20 equidistant values of θ and the same damping constant α for each individual spectrum. Since α does not influence significantly the FMR frequency, its effect on the simulated spectra is only to modify the FMR linewidth of individual spectrum. An increase of n did not change the values of α as a free parameter in the fitting procedure. Fig. 5.6 presents the fits based on this model of H_d.

In Table 5.2 we present the results of this analysis. We see that the amplitude of the demagnetizing field H_d increases clearly with the roughness. Like $\boldsymbol{H}_0$, $\boldsymbol{H}_{Shift}$ correlates with the roughness of the films and will be subject of discussion in the next section.

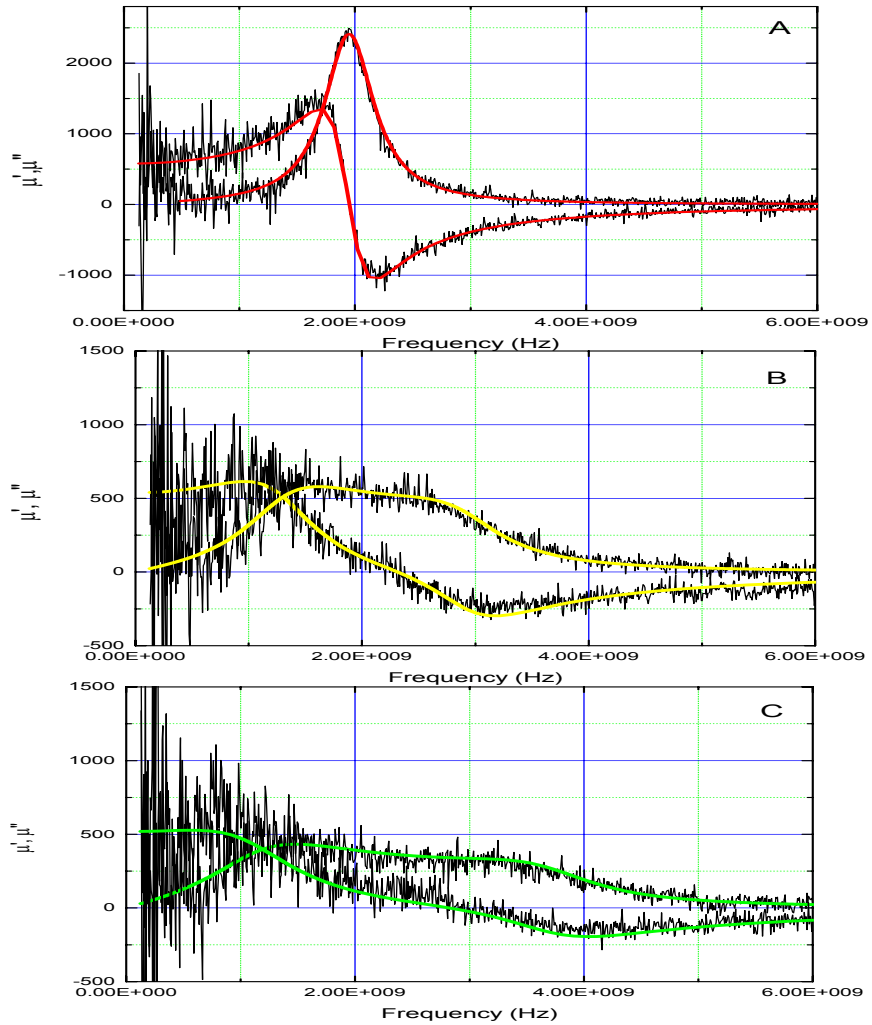

Fig. 5.6 Measurement and simulation of real and imaginary part of the complex permeability for sample A – (a), B – (b) and C – (c).

Method 2. We can also get an idea about the distribution of local demagnetizing fields by transforming spectra $\mu=\mu(f)$ into $\mu=\mu(H_{eff})$ via the dispersion relationship:

$$f_{H_{RF}||HA} = \frac{\gamma}{2\pi}\sqrt{4\pi M_S H_{eff}} \tag{5.8}$$

where $\gamma = \frac{g\mu_B}{\hbar}$ is the gyromagnetic ratio and μ_B is the Bohr magneton. The effective field acting on the spins is given by $H_{eff}=H_k+H_{Shift}+H_d$. If we neglect the intrinsic line-width with respect to the inhomogenous broadening of the resonance line the curve of μ' versus H_{eff} reflects the distribution of local fields H_d, see Fig. 5.7. This seems a reasonable assumption, because the linewidth for sample A is much narrower than for B and C. On the other hand, for a successful fit assuming a sine wave variation of H_d we had to introduce a much larger homogenous linewidth for samples B and C. So we may overestimate the width of the distribution by using method 2.

However, the large homogeneous linewidth used in method 1 may also be (partly) the consequence of the fact that the local field distribution is forced to be sinusoidal. We conclude that we have some evidence for an increased homogeneous linewidth in samples B and C, but no conclusive proof.

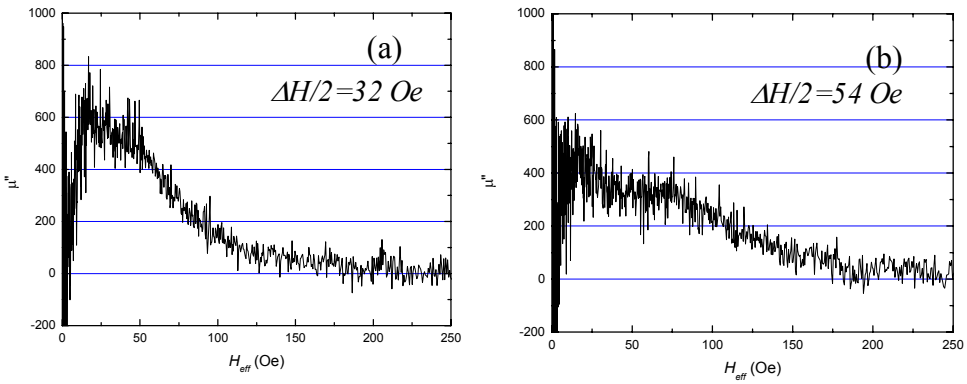

Fig. 5.7 $\mu''=\mu''(H_{eff})$ obtained directly from the dispersion relationship for the samples B-a and C-b.

Anyway, the two methods give quite comparable results. We see that the values of the half line widths are very close to those of $\boldsymbol{H_0}$ presented in Table 5.2. We also notice that the average field is much larger than H_K.

5.4. Discussion

Based on the interpretation given in section 5.3, we summarize the effects observed on the FMR absorption line: i) the line asymmetry, ii) the line position and iii) the homogenous line width as observed in the damping parameter.

Line shape

Our permeability measurements clearly show that there exists an asymmetric distribution of resonance frequencies. We ascribe this to a distribution in local demagnetizing fields, due to roughness of both film interfaces. In comparing with the AFM analysis, we have to realize that due to the strong exchange interactions, the spins are coupled over regions with an in-plane area proportional to the square of the magnetic correlation length ξ_m. In case of pure Fe, $\xi_m \approx 35$ nm, and we expect approximately the same number in our samples. Only the structural irregularities larger than ξ_m will lead to variations in the resonance frequency of the local magnetization, i.e. to inhomogenous line broadening. A proper comparison requires that we calculate N_{xx} (N_{zz}) by limiting the integration in eq. 5.4. to $k_{max} = 2\pi/\xi_m$.

Although a quantitative comparison is difficult, we expect that the average demagnetizing field $H_{zz}=N_{zz}4\pi M_S$ as calculated from the AFM profiles will be close to the halfwidth of the local field distribution (method 2) or, alternatively, to the amplitude of the sinusoidal variation H_0 (method 1). For sample B, the size of the hillocks L≅ 400nm is much longer than the magnetic correlation length, so that $H_{zz}=N_{zz}4\pi M_S \cong$ 15Oe is the appropriate estimate for the interface roughness. Given the very rough nature of this estimate, this is in agreement with the permeability estimates: 25Oe (method 1) and 32Oe (method 2). For sample C we have a lateral correlation length ξ =78 nm. It turns out that limiting the integration in eq. 5.4 to $k_{max}= 2\pi/\xi_m$ has a negligible influence on the the value of N_{zz}. The value $N_{zz}4\pi M_S =$ 55Oe compares well with the permeability estimates: 44 and 54Oe, respectively.

Line shift

Recently, Arias and Mills [18] proposed a model for thin films, based on scattering of the normal mode by bumps and pits on the sample surface or the interface. According to their interpretation, the shift effect may occur only if there is a *preferential* orientation of the surface imperfections. Contrary to this, we clearly observe a FMR line shift but we have no evidence for a preferential orientation of the surface defects. If we assume that the demagnetizing fields H_{xx} and H_{zz} are equal due

to the random character of the surface imperfections, their contribution in the general expression of the FMR frequency will cancel out:

$$f_R = \frac{\gamma}{2\pi}\sqrt{\left[H_k + \left(N_{xx} - N_{zz}\right)4\pi M_S\right]\left[H_k + \left(N_{yy} - N_{zz}\right)4\pi M_S\right]} \qquad (5.9)$$

We conclude that in this case the surface roughness does not lead to a shift of the FMR frequency.

As already discussed in chapter 4, the FMR frequency shift can be related to the variation of the magnitude of the magnetization due to the existence of grains and intergranular regions. The perpendicular magnetization component M_x can be associated with a magnetostatic energy density $<(M_x\text{-}M_{av,x})^2>$. Applying the simple model of Jamet and Malozemoff [19], which assumes a sinusoidal variation of the magnetization with amplitude M_1, we estimate $M_1 \approx 4.\ 10^2$ G for sample A and $9.\ 10^2$G for samples B and C. These values are 2.5%, resp. 6% of the saturation magnetization. Probably the rougher surface topography of substrates B and C leads to a rougher film structure, with larger density (magnetization) fluctuations.

Spin wave excitation

The damping constants as determined from the X-band measurements (α_{field}) and from the permeability spectra ($\alpha_{frequency}$) are presented in table 2. For the same sample the values calculated from the permeability spectra are larger than those obtained from the FMR measurements. (In fact the difference is even more pronounced, because we did not take inhomogenous broadening into account in the X-band measurements, whereas we did so in the permeability analysis via the parameter H_0). In addition we observe that $\alpha_{frequency}$ and α_{field} increase with the sample roughness.

In the framework of the two magnon scattering process, the homogenous broadening of the resonance line is associated with the presence of spin waves with the same energy as the uniform precession mode. The uniform precession mode is scattered by randomly distributed inhomogeneities into these spin wave modes. As a consequence the damping parameter α will increase (above its intrinsic value) with the number and the volume of the magnetic inhomogeneities. This interpretation is widely accepted [20]. In our case the structural imperfections in the bulk and the surface can be considered as scattering centers in the two-magnon process. The fact that for $\boldsymbol{H_{DC}}$ oriented in the plane the uniform FMR mode is degenerate with the whole spin wave band is reflected in the damping parameter evolution from small values for sample A to (presumably) very large values for sample C. The decrease of α when going to higher frequencies (higher effective fields) is similar to what observed in Chapter 4, but presently not understood. We refer to this chapter for more details.

5.5. Conclusions

We have demonstrated that the high frequency magnetic response can be influenced by changing the roughness of the substrate. It turns out that both the shift and the broadening of the resonance line can be understood from the roughness of the film interfaces. The estimations of the demagnetizing field as calculated from the analysis of AFM scans are reasonably close to the values of the halfwidth of the local field distribution, obtained from the FMR frequency-dependent measurements.

A possible route of further investigations is to continue this study on thin films deposited on patterned substrates obtained, for instance, by laser interference lithography [22]. In this way the magnitude of the local demagnetizing field can be controlled in an easier manner. Complementary, FMR field dependence measurements, realized with the external applied field oriented perpendicular to the sample surface would be quite interesting. Because in such a geometry the two magnon scattering process is absent, it could yield the final proof that we have an unusual large damping constant in our samples.

References

1. M. Yamaguchi, K. Suezawa, K. I. Arai, Y. Takahashi, S. Kikuchi, Y. Shimada, W. D. Li, S. Tanabe, K. Ito, J. Appl. Phys. **85**, 7919 (1999).
2. M. Yamaguchi, M. Baba, K. I. Arai, IEEE Trans. On Microwave Theory and Techniques **49**, 2331 (2001).
3. G. Herzer, IEEE Trans. on Magn. **26**, (1990) 1397.
4. R. Alben, J. Becker, and M. C. Chi, J. Appl. Phys. **49**, 1653 (1978); E. M. Chudnovsky, W. M. Saslow,and R. A. Serota, Phys. Rev. B **33**, 251 (1986).
5. A. R. Chezan, Nanostructure and soft magnetic properties of iron-nitrogen alloys, Thesis, University of Groningen, The Netherlands.
6. J.F. Bobo, H. Chatbi, M. Vergnat, L. Hennet, O. Lenoble, Ph. Bauer, M. Piecuch, J. Appl. Phys. **77**, 5309, (1995).
7. D. Pain, M. Ledieu, O. Acher, A.L. Adenot, F. Duverger, J. Appl. Phys. **85**, 5151, (1999). See also Chapter 2 for more details.
8. J. Krim and G. Palasantzas, Int. J. of Mod. Phys. **B9**, 599 (1995); Y. P. Zhao, G. -C. Wang, and T. -M. Lu, *Characterization of amorphous and crystalline rough surfaces-principles and applications*, (Experimental Methods in the Physical Science Vol. 37, Academic Press, 2000); P. Meakin, *Fractals, Scaling, and Growth Far from Equilibrium* (Cambridge University Press, Cambridge, 1998); T. Halpin-Healy, Phys. Rep. **254**, 215 (1995).
9. Z. P. Zhao, G. Palasantzas, G. -C. Wang, and J. Th. M. De Hosson, Phys. Rev. B **60**, 1216 (1999); G. Palasantzas, J. Appl. Phys. **86**, 2196 (1999).
10. G. Palasantzas, Phys. Rev. B **48**, 14472 (1993); **49**, 5785 (1994).
11. G. Palasantzas and J. Krim, Phys. Rev. B **48**, 2873 (1993); G. Palasantzas, Phys. Rev. E **49**, 1740 (1994); S. K. Sinha, E. B. Sirota, S. Garoff, and H. B. Stanley, Phys. Rev. B **38**, 2297 (1988); H.-N. Yang and T.-M. Lu, Phys. Rev. E **51**, 2479 (1995).
12. E. Schlömann, J. Appl. Phys. **41**, 1617 (1970).
13. S. Chikazumi, Physics of Ferromagnetism, Oxford university Press, (1997).
14. L. Landau, E. Lifshitz, Physik. Z. Sowjetunion **8**, 163 (1935).
15. E van de Riet, W. Klaassens, F. Roozeboom, J.Appl.Phys, **81**, 806 (1997); see also the Chapter 4 of this thesis.
16. J. Huijbregtse, F. Roozeboom, J. Sietsma, J. Donkers, T. Kuiper, and E. Van de Riet, J. Appl. Phys. **83**, 1569 (1998).
17. C. J. Oates, F. Y. Ogrin, S. L. Lee, P. C. Riedi, G. M. Smith, T. Thomson, J. Appl. Phys. **91**, 1417 (2002).

18. R. Arias, and D. L. Mills, Phys. Rev. B **60**, 7395 (1999).
19. J.P. Jamet and A.P. Malozemoff, Phys. Rev. B **18**, 75 (1978).
20. M. Sparks, R. Loudon, and C. Kittel , Phys. Rev. 122, 791 (1961).
21. C.B. Craus, A.R. Chezan, N. G. Chechenin, D.O. Boerma, L. Niesen, submitted to Phys. Rev.B
22. J. C. Lodder, M. A. M. Haast, and L. Abelmann, Magnetic Storage Systems Beyond 2001, Kluwer Academic Publishers, Dordrecht, The Netherlands, 117 (2001)